The impact of radiation feedback on the assembly of star clusters in a galactic context

Nicolas Guillard, Eric Emsellem, Florent Renaud

Monthly Notices
of the
ROYAL ASTRONOMICAL SOCIETY

MNRAS **477,** 5001–5010 (2018) doi:10.1093/mnras/sty849

The impact of radiation feedback on the assembly of star clusters in a galactic context

Nicolas Guillard,[1,2]★ Eric Emsellem[2,3] and Florent Renaud[4,5]

[1]*Excellence Cluster Universe, Boltzmannstrasse 2, D-85748 Garching, Germany*
[2]*European Southern Observatory, Karl-Schwarzschild-strasse 2, D-85748 Garching, Germany*
[3]*Université de Lyon 1, CRAL, Observatoire de Lyon, 9 avenue Charles André, F-69230 Saint-Genis Laval; CNRS, UMR F-5574; ENS de Lyon, France*
[4]*Department of Physics, University of Surrey, Guildford GU2 7XH, UK*
[5]*Lund Observatory, Department of Astronomy and Theoretical Physics, Box 43, SE-221 00 Lund, Sweden*

Accepted 2018 March 29. Received 2018 March 29; in original form 2017 October 2

ABSTRACT

Massive star clusters are observed in galaxies spanning a broad range of luminosities and types, and are assumed to form in dense gas-rich environments. Using a parsec-resolution hydrodynamical simulation of an isolated gas-rich low-mass galaxy, we discuss here the non-linear effects of stellar feedback on the properties of star clusters with a focus on the progenitors of nuclear clusters. Our simulation shows two categories of star clusters: those for which feedback expels gas leftovers associated with their formation sites, and those, in a denser environment, around which feedback fails to totally clear the gas. We confirm that radiation feedback (photoionization and radiative pressure) plays a more important role than Type II supernovae in destroying dense gas structures, and in altering or quenching the subsequent cluster formation. Radiation feedback also disturbs the cluster mass growth, by increasing the internal energy of the gas component to the point at which radiation pressure overcomes the cluster gravity. We discuss how these effects may depend on the local properties of the interstellar medium, and also on the details of the subgrid recipes, which can affect the available cluster gas reservoirs, the evolution of potential nuclear cluster progenitors, and the overall galaxy morphology.

Key words: methods: numerical – ISM: structure – Galaxy: evolution.

1 INTRODUCTION

Most stars seem to form in cluster environments (Lada & Lada 2003; Mac Low & Klessen 2004). In the Milky Way, ∼70 per cent of spectral O-type stars are located in young clusters or associations (Gies 1987; Parker & Goodwin 2007). In nearby starburst galaxies, young star clusters are strong ultraviolet (UV) emitters and the sources of at least 20 per cent of UV light (Meurer et al. 1995). Star clusters hence represent key components of star formation in galaxies, play an important role in the formation and evolution of their host, and connect the physics of the interstellar medium (ISM), star formation and feedback. The formation and evolution of star clusters represent a challenge for models and simulations because of the complex coupling between various spatial scales and physical processes (e.g. Li, de Grijs & Deng 2016; Naab & Ostriker 2017; Niederhofer et al. 2016; Chatterjee, Rodriguez & Rasio 2017; Bekki 2017; Lamers et al. 2017). At the massive end, the build-up of clusters requires sufficiently high gas densities, such as those that exist in the Local Group, for instance in starbursts (Portegies Zwart, McMillan & Gieles 2010, Longmore et al. 2014). Such extreme conditions are expected to be more frequent at high redshifts, when the gas fraction of galaxies was high (50 per cent and above, see Daddi et al. 2010).

Such gas-rich environments provide favourable conditions for the assembly of massive clusters and in particular for the seeds of the most massive clusters, the nuclear clusters (NCs). Observed at or near the centre of a wide variety of galaxies of all Hubble types (e.g. Carollo, Stiavelli & Mack 1998; den Brok et al. 2014), NCs are among the densest objects in the Universe, with masses from 10^5 $M_\odot$ to 10^8 $M_\odot$ and typical radii of a few parsecs. They are also characterized by multiple stellar populations, spanning ages from 10 Myr to more than 10 Gyr (e.g. Lee et al. 1999; Rossa et al. 2006; Seth et al. 2006; Perets & Mastrobuono-Battisti 2014). The main formation scenarios for NCs are nuclear inflows of gas leading to in situ formation (Milosavljević 2004), the dry-merger of clusters (Tremaine, Ostriker & Spitzer 1975), or a combination of the two (Guillard, Emsellem & Renaud 2016). It is still unclear, however, how these scenarios relate to the properties of the galactic host.

The formation of NCs is a complex problem that relies on the coupling of several physical processes (e.g. star formation and stellar feedback) occurring in environments with extreme physical

★ E-mail: nguillar@eso.org

properties. It is presumed that at the time of their formation (up to 10 Gyr ago, see Cole & Debattista 2016 and references therein) gas was abundant within the galactic disc, a condition that is favourable for the formation of star clusters (e.g. Arca-Sedda et al. 2015). Guillard et al. (2016), for example, showed the importance of gas reservoirs of young clusters in the formation and growth of NCs. Such reservoirs are expected to be significantly perturbed by, for example, stellar feedback.

Stellar feedback and its effect within galaxies have been studied extensively over the years (Hopkins et al. 2014, 2017; El-Badry et al. 2016; Nelson et al. 2015; Bournaud et al. 2010; MacLachlan et al. 2015; Krumholz et al. 2014; Raskutti, Ostriker & Skinner 2016; Howard, Pudritz & Harris 2016; Grisdale et al. 2017). Such studies have focused on a variety of spatial scales and physical processes. For example, at parsec (pc) and subparsec scales, numerical works have investigated the role of photoionization (Dale, Ercolano & Bonnell 2012; Walch et al. 2012; Tremblin et al. 2014; Geen et al. 2016) and stellar winds (Wareing, Pittard & Falle 2017; Rey-Raposo et al. 2017) in the life of molecular clouds and in the star formation within them. The model of feedback implemented by Núñez et al. (2017) in simulations of an isolated Milky Way using various physical principles (stellar winds from young massive stars, heating by massive stars within Strömgren spheres, and a limiting-cooling mechanism based on the recombination time of dense H II regions) showed that star formation is more extended (in time and space) when all these physical mechanisms are used simultaneously than when pure thermal supernova (SN) feedback is used. Agertz et al. (2013) also showed that pre-SN feedback (i.e. radiative pressure and stellar winds) is efficient at clearing the gas away from star-forming regions, thus making the subsequent heating from SNe even greater. Regarding kiloparsec scales, other studies have shown that stellar feedback is associated with violent events such as molecular outflows (Geach et al. 2014; Hayward & Hopkins 2017) and helps to shape the gaseous content of galaxies (Agertz & Kravtsov 2015, 2016). Because feedback acts directly or indirectly from subparsec to kiloparsec scales, it was difficult for dedicated hydrodynamical simulations to both cover the full spatial range and extend over long time-scales (Gyr). Moreover, most of these studies are based on conditions that are observed in the Local Universe, and it is thus still unclear how stellar feedback affects the ISM and the formation regions of star clusters in gas-rich discs. With present-day supercomputers, however, we can start to address these issues and the impact of stellar feedback from parsec to kiloparsec scales.

Different feedback mechanisms are expected to play different roles in regulating the assembly of star clusters, and their non-linear interplay makes the matter even more complex to study. The aim of the present paper is to examine their relative contributions and to determine how they influence the properties of young star clusters. Addressing these topics will allow us to better understand the direct impact that stellar feedback has on the properties of the gas, and consequently on the properties of star clusters when they first form (seeds) and evolve (e.g. as they grow and merge). The context of this study will be that of an isolated gas-rich galaxy. We choose to focus on a galactic stellar mass of about $10^9\,M_\odot$, as this corresponds to the peak of the fraction of nucleated discs (Pfeffer et al. 2014). With such a setup, we extend the study of Guillard et al. (2016), which will serve as a reference. In order to understand better the role of feedback, we use the same set of feedback recipes as in Guillard et al. (2016), switching off all or part of the feedback components in turn, and comparing the properties of the forming and evolving star clusters. The physics recipes and initial conditions we employ in the present paper are similar to those of the reference simulation. In Section 2, we briefly describe the numerical methods. In Section 3, we compare the properties of the star cluster population when feedback is active and when it is not. We provide a discussion and some conclusions in Section 4.

2 NUMERICAL METHODS

In this paper, we present numerical simulations that use initial conditions and prescriptions similar to those in Guillard et al. (2016). Hence we present here only a summary, and refer the reader to Guillard et al. (2016) for further details. We conducted hydrodynamical simulations of an isolated gas-rich dwarf galaxy with the adaptive mesh refinement (AMR) code RAMSES (Teyssier 2002). The code solves the Euler equations on the AMR grid with a maximum refinement of 3.7 pc in the densest gaseous regions of the $(30\,\mathrm{kpc})^3$ volume. The least-resolved cells span 120 pc. The code ensures that the Jeans length is always resolved by at least four cells. A particle-mesh scheme is used to solve the equations of motion, with a softening of 7 pc for the gravitational acceleration of the particles coming from the initial conditions (namely the dark matter and the stars included in the initial conditions) and a minimum of 3.7 pc for the stellar particles formed during the simulations (hereafter stars, for simplicity), which corresponds to the local finest refinement of the AMR grid. The simulations were run on the C2PAP facilities (Excellence Cluster, Garching) for about 1 million CPU-hours on 512 cores.

The isolated gas-rich dwarf galaxy that we simulate has a stellar mass of $10^9\,M_\odot$, a gas disc with a gas mass fraction of 70 per cent of the baryonic mass, and a Navarro–Frenk–White (Navarro, Frenk & White 1996) dark matter (DM) halo component. The latter has a mass of $10^{11}M_\odot$, which follows the scaling relationship between DM haloes and stellar discs in Ferrero et al. (2012), a concentration of 16 and a virial radius of 120 kpc. We truncate the halo at a radius of 15 kpc, thus focusing on the central regions of the galaxy. Both our stellar and our gaseous disc have a radial and a vertical exponential profile with a scaling radius of 1 and 1.65 kpc (respectively) and a scaleheight of 250 and 165 pc (respectively).

Our simulations use the same recipes for star formation and stellar feedback as in Renaud et al. (2013). Star formation occurs when the gas reaches a density higher than $100\,\mathrm{cm}^{-3}$. The gas is then converted into stars with an efficiency of 2 per cent per free-fall time. These stars have a mass M_* of $130M_\odot$. We then model stellar feedback coming from these newly formed stars with three processes: photoionization, which creates H II regions; radiative pressure (Renaud et al. 2013); and Type II supernovae (Dubois & Teyssier 2008). In more detail, the radius of the H II region is

$$r_{\mathrm{HII}} = \left(\frac{3}{4\pi}\frac{L_*}{n_\mathrm{e}^2\alpha_\mathrm{r}}\right)^{1/3}, \quad (1)$$

where L_* is the luminosity of the central stellar source, and n_e and α_r are the density of electrons and the recombination rate, respectively. Within each of these bubbles, we set the gas to have a uniform temperature of 4×10^4K, a value that is significantly higher than the temperature of the surrounding warm ISM. Although this temperature is a few times higher than the typical observed value (e.g. Lopez et al. 2011), we checked that this difference does not affect our conclusions. The ionization of the ISM is treated as follows: to speed-up the computation, one out of every 10 stars radiates and ionizes the surrounding ISM with an energy 10 times higher than a single source. Considering that star formation occurs in dense gas regions in clusters, this treatment ensures that all of

these regions contain at least one bubble. The luminosity is then

$$L_* = L_0 M_* \eta_{\rm OB} \begin{cases} 1 & \text{for } t_{\rm ff} < a_* \leq 4\,\text{Myr}. \\ (4\,\text{Myr})/a_* & \text{for } 4\,\text{Myr} < a_* < 10\,\text{Myr}. \\ 0 & \text{otherwise}, \end{cases} \quad (2)$$

where $L_0 = 6.3 \times 10^{46} \text{s}^{-1} \text{M}_\odot^{-1}$, M_* is the mass of the star that was spawned $a_{\rm star}$ is the age of the source, $\eta_{\rm OB} = 0.2$ is the stellar mass fraction that explodes into SNe, and $t_{\rm ff}$ is the local free-fall time (see e.g. Leitherer et al. 1999). If two H II regions overlap, the code ensures that the ionized volume is conserved and merges the two bubbles if the separation between them is smaller than their radii. Finally, the momentum feedback, which here is carried by H II regions, is injected in the form of velocity kicks and is proportional to L_* (see Renaud et al. 2013 for details):

$$\Delta v = s \frac{L_* h \nu}{M_{\rm HII} c} \Delta t, \quad (3)$$

where h is the Planck constant, $M_{\rm HII}$ is the gas mass of the bubble, c is the speed of light, and ν is the frequency of the flux representative of the most energetic part of the spectrum of the source. We consider here the luminosity of the Lyman α and set $\nu = 2.45 \times 10^{15} \text{s}^{-1}$. s is a dimensionless parameter accounting for the multiple electron scattering through the bubble and the decay of energy between each collision. We set $s = 2.5$ as in Renaud et al. (2013).

Our stars explode as SNe after 10 Myr. The SNe are modelled as Sedov blasts (see Dubois & Teyssier 2008). The initial radius of the ejecta is 10 pc. The total mass removed from each cell affected by the blast wave when the SN explodes is $M_*(1 + \eta_{\rm OB} + \eta)$, where η is the mass-loading factor for the winds. The mass-loading factor η sets the allocation of the momentum between its mass and velocity terms. SNe inject 10^{51} erg of energy in kinetic form, and the energy released to the gas by the debris is $E_{\rm d} = \eta_{\rm OB}(M_*/M_{\rm SN})E_{\rm SN}$, where $M_{\rm SN}$ and $E_{\rm SN}$ are respectively the typical progenitor mass and the energy of an exploding Type II supernova (i.e. 10^{51} erg). The initial Sedov blast wave propagates at a velocity given by

$$u_{\rm Sedov} = \frac{\sqrt{2}}{5} \left[f_{\rm ek} \eta_{\rm OB} \left(\frac{\delta x}{\Delta x} \right)^3 \frac{1}{1 + \eta_{\rm OB} + \eta} \right]^{1/2} u_{\rm SN}, \quad (4)$$

where $f_{\rm ek} = 0.05$, δx^3 is the volume of the cell in which the explosion occurs, Δx is the radius of the shock from the centre of the explosion, and $u_{\rm SN}$ is the velocity corresponding to the kinetic energy of one SN explosion. The momentum of the blast wave is then added to that of the gas.

Finally, we use the friend-of-friend algorithm 'HOP' (Eisenstein & Hut 1998) to detect star clusters. The density thresholds for detection are the same for all simulations and are as in Guillard et al. (2016). Namely, a cluster is detected when the peak of the local stellar density exceeds $1.5\,\text{M}_\odot\,\text{pc}^{-3}$, with an outer boundary limit of $0.5\text{M}_\odot\,\text{pc}^{-3}$ to prevent the detection of stars in the field. Two clusters are merged if the saddle density between them is higher than $1\text{M}_\odot\,\text{pc}^{-3}$.

3 STELLAR FEEDBACK AND THE STAR CLUSTER POPULATION

In this section, we examine how the star cluster populations are affected by feedback in our simulations. We thus present the results of test simulations for which individual feedback mechanisms are turned on or off.

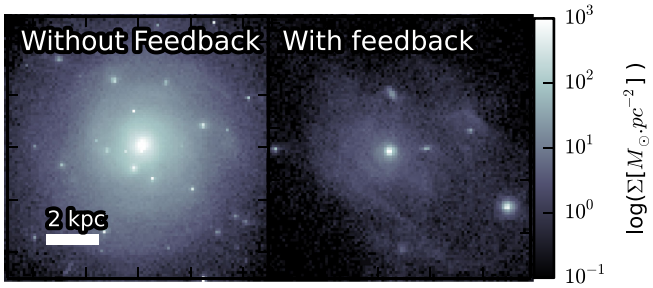

Figure 1. Face-on surface density of the stars formed during the simulations without (left) and with (right) feedback. The displayed galaxies have evolved for 940 Myr. The star cluster population is different for the two cases: without feedback, a massive nucleus forms, surrounded by several tens of smaller and less dense clusters, while with feedback, only five clusters orbit around a nuclear cluster.

3.1 The star cluster populations

We first choose to compare two sets of simulations: one from Guillard et al. (2016), which includes all the above-mentioned feedback recipes (see Section 2), and another with the same initial conditions but for which feedback is not active from the start.

Fig. 1 illustrates the difference in the star cluster populations after 940 Myr of evolution between these two simulations. After nearly 1 Gyr of evolution, the star cluster population is already well established in both cases. At this time, the galaxies no longer host dense gas clouds, preventing the formation of additional star clusters.

The simulation without feedback exhibits 78 clusters at $t = 940$ Myr, with a massive central cluster of $\sim 6 \times 10^8 \text{M}_\odot$, and has formed hundreds of clusters over that period. Most of these clusters (~90 per cent) formed during the first 50 Myr after the trigger of star formation (at $t = 80$ Myr). This contrasts strongly with the outcome of the simulation when feedback is active: only six clusters, including the nuclear cluster, are observed at $t = 940$ Myr. The subsequent evolution during the next Gyr is again insignificant, with no drastic change in the cluster population: two clusters are destroyed by cluster–cluster interactions, and the nuclear cluster experiences a merger at $t = 1.7$ Gyr (see Guillard et al. 2016 for details).

When feedback is active, it can be seen that there is a lack of star clusters with mass lower than $10^5 \text{M}_\odot$ at $t = 940$ Myr (see Fig. 2): such low-mass clusters are detected at some point (see the stacked distribution in Fig. 2) but either are systematically destroyed by cluster–cluster interactions or merge into more massive clusters, leaving this low-mass bin empty at $t = 940$ Myr. It is also worth noting that there are populations of young stars that accumulate in various regions of the disc, but these associations (with stellar densities below our detection threshold) are dispersed by stellar feedback and local variations in the local gravitational potential. This contrasts with the simulation without feedback, which contains a few tens of such low-mass star clusters. These clusters are located in the outer regions of the disc and do not interact with one another. This allows the clusters with the lowest mass to survive for more than 2.5 Gyr.

The nucleus in the no-feedback run is 10 times more massive ($5 \times 10^8 \text{M}_\odot$) than that of the reference simulation ($\sim 5 \times 10^7 \text{M}_\odot$). This is a direct consequence of both the higher merger rate in the former case (11 mergers for the no-feedback case) and the higher in situ star formation rate owing to the absence of feedback. These mergers supply the nucleus with stars but also with gas, which is

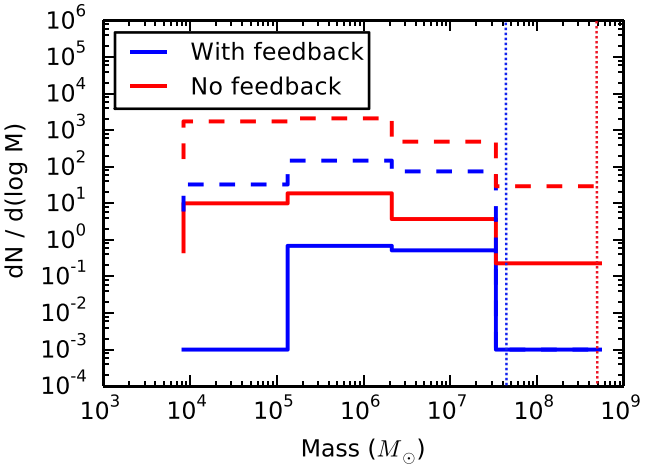

Figure 2. *Solid*: The cluster mass function (CMF) for the simulations with (blue) and without (red) feedback at $t = 940$ Myr. The dotted lines mark the mass of the nuclei in both simulations. We note that these distributions suffer from low-number statistics. *Dashed*: CMF stacked over 940 Myr; that is, for each output between $t = 0$ and $t = 940$ Myr (with an average frequency of 1 output every 5 Myr) we calculated the CMF and summed them over that period. The low-mass end of the CMFs break at $10^4 M_\odot$ owing to the lower limits of the density detection thresholds. It can be seen that at $t = 940$ Myr, clusters with a mass below $10^5 M_\odot$ are not observed when feedback is active. The stacked CMF shows that such cluster populations existed during the evolution but were either destroyed or grew into more massive clusters.

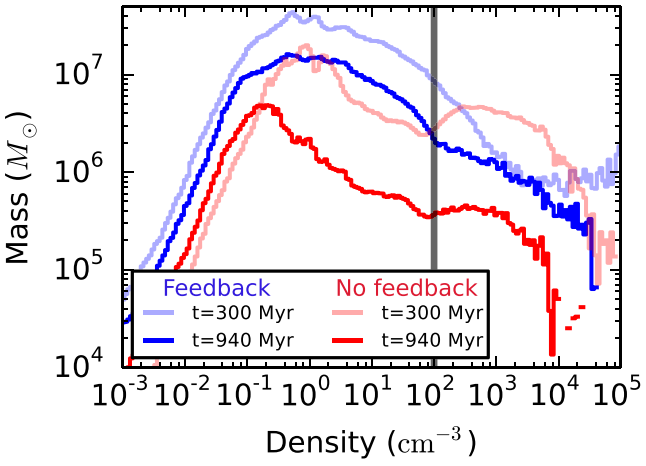

Figure 3. Probability distribution function of the gas density for simulations with (blue) and without (red) feedback within the galaxy at various times (shown in the legend). The vertical line marks the star formation threshold. At $t = 940$ Myr, less gas is detected in the simulation without feedback than it is when feedback is included. This is because of the higher star formation rate (above $1 M_\odot \mathrm{yr}^{-1}$)

brought with the incoming clusters. Such events occur only twice in the reference simulation because of the limited number of clusters. Other surviving clusters of that simulation are gas-free within 10–20 Myr and their mass does not evolve thereafter.

3.2 The effect on dense gas

The different formation rates of the clusters for the two cases (15 clusters in 940 Myr with feedback and 320 without feedback) can be interpreted as a direct consequence of the effect of feedback on the availability of dense gas throughout the disc. Fig. 3 displays the evolution of the probability distribution function (PDF) of the gas density at different times in the life of the two simulated low-mass galaxies.

When feedback is on, the PDF has a log-normal shape for gas densities below $100\,\mathrm{cm}^{-3}$, with a peak at $\rho = 1\,\mathrm{cm}^{-3}$. For higher densities, the shape of the PDF is that of a power law, with a possible mass excess above $3 \times 10^3\,\mathrm{cm}^{-3}$ (e.g. at $t = 300$ Myr) corresponding to the central regions of the gas reservoir of the most massive clusters. Such a power-law tail has been interpreted as a convolution of the classical log-normal shape from the turbulent gas with that of the self-gravitating gas clouds (Audit & Hennebelle 2010; Renaud et al. 2013). As time progresses, dense gas is consumed to form stars, while part of the less-dense gas cools down and evolves towards a higher density, lowering the relative weight of the log-normal part of the PDF. At $t = 940$ Myr, the nuclear cluster has formed, and the power-law seen in Fig. 3 is associated with the cluster's self-gravitating gas reservoir. The excess of mass in the highest-density bin disappears owing to the central star formation, which consumes dense gas, and the subsequent gas dispersion induced by stellar feedback.

The major difference between the simulations with and without feedback occurs around the star formation threshold at $100\,\mathrm{cm}^{-3}$. When there is no feedback, a sharp transition is observed at this density, with a lack of gas at lower densities and an accumulation of gas with density between 100 and $300\,\mathrm{cm}^{-3}$. A comparison with the simulation with feedback, which displays a smoother transition at $100\,\mathrm{cm}^{-3}$, confirms that feedback redistributes dense gas towards lower densities (see e.g. Grisdale et al. 2017 and references therein). This redistribution thus leads to a relative lack of dense gas, which could have been used to form stars in general and star clusters in particular. Overall, the gas redistribution induced by the stellar-driven feedback towards low densities is responsible for the smaller number of clusters. This redistribution of dense gas is also responsible for the non-growth mass of star clusters in our simulation with feedback, with the exception of two clusters that manage to keep their reservoir (see the following sections). It is also important to note that the absence of stellar feedback does not inhibit the accumulation of dense gas in the disc, because only thermal pressure can oppose the collapse of the clouds. In the next section, we focus on the processes involved in this redistribution and how they affect the growth of star clusters.

3.3 Radiative versus supernova feedback

In the previous sections, we saw that adding stellar-driven feedback changes, as expected, the properties of the ISM and, consequently, that of the star cluster population. In this section, we further investigate how individual feedback processes impact the growth of star clusters.

We address this question by running two additional simulations for which we single out SN feedback on the one hand and radiative feedback (H II regions + radiative pressure) on the other. We start with an actual population of star clusters, hence following the mass distribution properties illustrated in Fig. 2, and then focus on the subsequent evolution depending on the implemented feedback schemes. Fig. 4 illustrates the long-term impact of these recipes by showing the face-on density maps of the gas with the positions of all star clusters detected at $t = 600$ Myr (about 500 Myr after star formation is triggered).

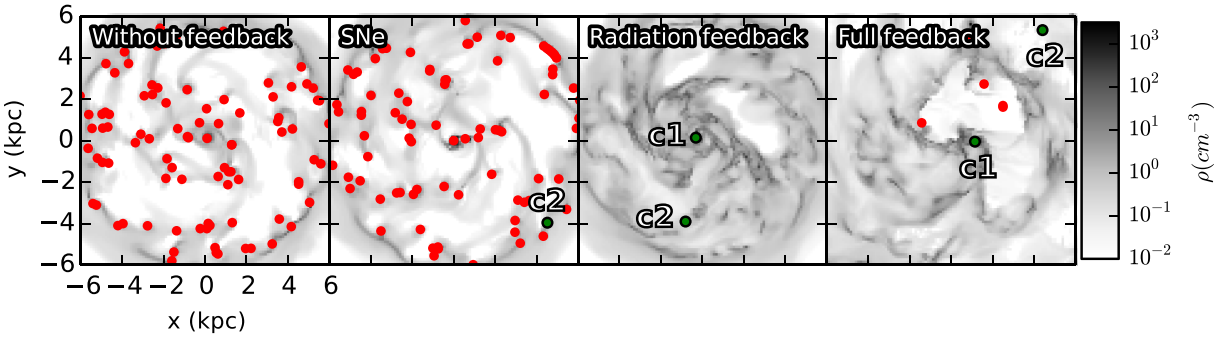

Figure 4. Face-on density maps of the gas at $t = 600$ Myr for simulations using different setups for stellar feedback: without feedback (left), SNe only (middle-left), H II regions + radiative pressure (middle-right) and SNe + H_{II} regions + radiative pressure (right). The cases with full feedback and without feedback are the same as those discussed in the previous sections. The densities are averaged on 1 kpc along the line of sight. The initial conditions are the same for all simulations. Red circles show the positions of star clusters. Green circles are the clusters for which the early evolution will be studied in Fig. 5 and Section 3.4. Clusters labelled as C1 keep their gas reservoir, whereas those labelled as C2 expel their gas during the first 10 Myr after formation. Star cluster populations in the no-feedback and SN-only cases are similar in terms of number and individual mass. When radiative feedback is included, the interstellar medium becomes less clumpy and the formation of clusters is reduced. The heating from H II regions and radiative pressure redistribute the gas towards lower densities and slow down the formation of massive clumps from which star clusters could emerge.

The addition of feedback only from SNe does not seem to significantly alter the morphology of the ISM on large scales, or the cluster population, compared with the no-feedback simulation. The energy coming from SNe locally increases the temperature of the surrounding gas. Here, SNe are located in dense gaseous regions. Without any mechanisms (e.g. ionization) to disperse such dense gas before the SN explosions, the impact of SNe might be expected to be lower on the local environment (e.g. Agertz et al. 2013). Hence, the gas located in dense regions manages to cool down on very short time-scales (∼1 Myr), leaving most of the dense gas clouds intact. As a result, the seeds for star clusters are not greatly affected by SNe, and their populations are similar in the two cases (with or without SN feedback) in terms of mass and number. This result was also observed at subparsec scales by Rey-Raposo et al. (2017), who showed that SNe locally heat the gas, which cools down very rapidly, causing less impact on clouds than stellar winds. We checked that the properties of the ISM are not affected by the mass-loading factor of the winds (i.e. the amount of gas carried in SN debris). Using a mass-loading of unity, which impacts a higher gas mass but with smaller velocities, we observe no major differences for the PDF of the gas density or the cluster population in terms of number, size and mass. This suggests that the SNe are not the main actors altering the gas content of cluster-forming regions. In Section 4 we will discuss the impact of the numerical resolution and implementation on this result (see also e.g. Smith, Sijacki & Shen 2018).

Major differences arise when radiative feedback is activated: the ISM is less clumpy and more turbulent than in the no-feedback or SN-feedback cases, with more gas at densities between 1 and 100 cm^{-3} (of the order of $5 \times 10^8 M_\odot$ at $t = 600$ Myr over the entire galaxy). This suggests that the redistribution of the gas towards lower densities (see Section 3.2) is driven mainly by the radiation from H II regions. This leaves less dense gas from which massive star clusters can form, which in turn leads to a lower massive star cluster formation rate: only tens of clusters are formed over 500 Myr (a few clusters are observed at $t = 600$ Myr), as compared again to the hundreds in the simulations without feedback or with SN-only feedback within the same time range. Similar observations can be made with the simulation using all feedback recipes.

3.4 The ability of clusters to grow

Radiative feedback also affects the growth in mass of star clusters. There are two ways a cluster can gain mass: using a local gas reservoir to convert dense gas into stars or through mergers with other clusters. Because the number of mergers is low in simulations using radiative feedback, we focus here on growth by gas supply. Such a process of gas re-accretion occurs in two clusters in our simulations using radiative feedback, with the remaining clusters losing this reservoir a few million years after their formation. Their ability to retain and accrete more of their gas depends on the balance between the gravitational potential of the cluster (i.e. its stellar and gaseous components) and the energy of the gas (internal and injected by feedback). Assuming that the systems are in isolation, this balance can be estimated by comparing the total gravitational potential energy of the cluster with the internal energy (which we define here as the sum of the kinetic and the thermal energy) of the gas at a given time (thus ignoring the contribution from, for example, tidal fields).

We select a few clusters from the simulations with full, radiative (H II + radiative pressure) and SN feedback, respectively. In the former two cases, we choose one cluster that retains its gas for more than 20 Myr (respectively labelled as cluster Full-C1 and Rad-C1, also marked in Fig. 4), and one that expels its gas (respectively labelled as Full-C2 and Rad-C2). The C1 clusters are the NC progenitors. The C2 clusters in the SNe and radiation feedback simulations have an initial (i.e. at the time of their first detection) stellar mass density of the order of $4 M_\odot$ pc^{-3} within the inner 25-pc radius, with a slightly higher density for the cluster Full-C2 of $10 M_\odot$ pc^{-3}, owing to an initially more massive dense gas component in this region. In the simulation with SNe only, we do not observe clusters that expel their gas after their formation. We thus chose a cluster (SNe-C2) with an initial stellar density similar to that of the C1 and C2 clusters. All these clusters are shown in green in Fig. 4 .

We follow all these clusters over their first 50 Myr. We also limit our estimations of the energies to the inner 25 pc around the cluster and systematically check that only one stellar dense structure is included. We then measure and plot the ratio of the internal energy of the gas to the total gravitational potential energy of the clusters, alongside their stellar and gaseous masses, which we present

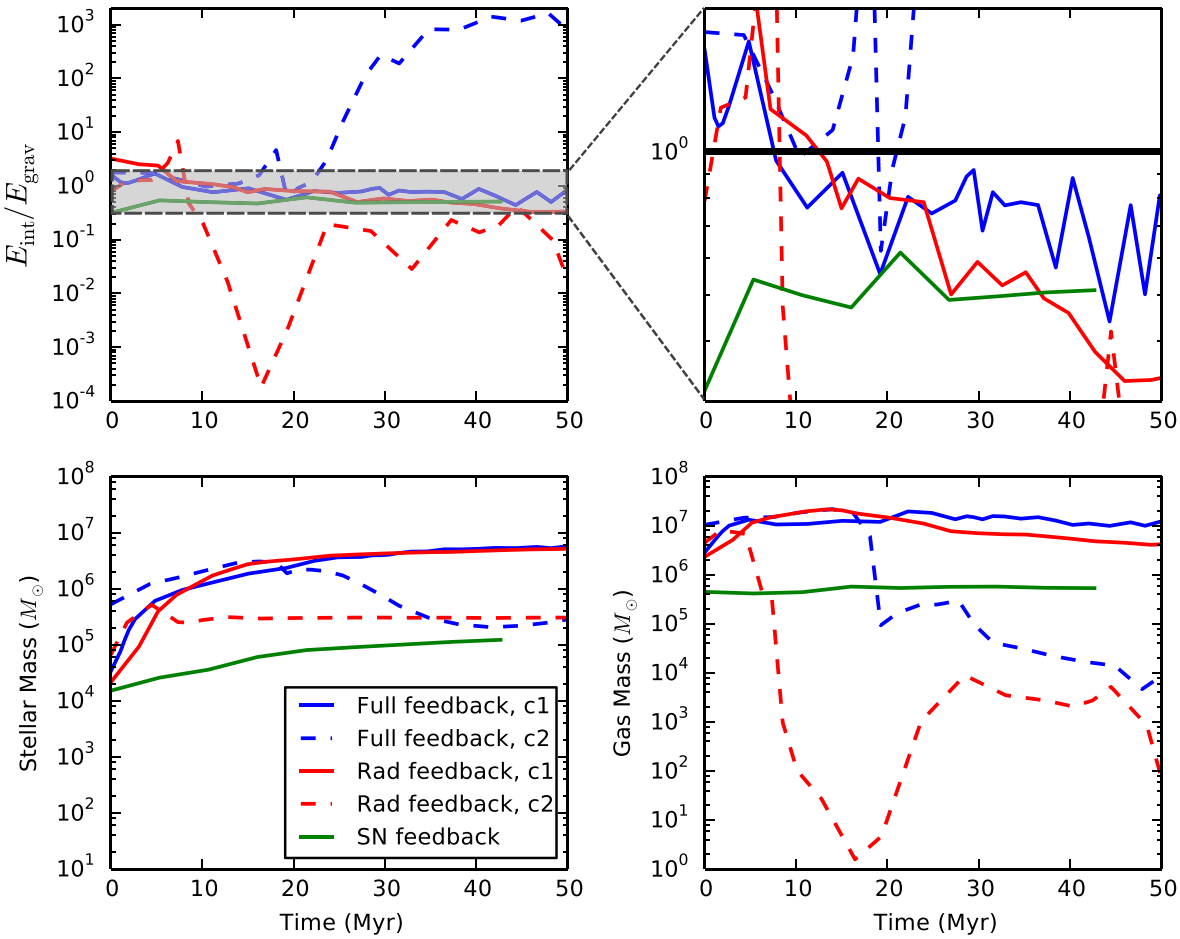

Figure 5. *Top*: Evolution of the ratio of the internal energy of the gas to the gravitational energy of the cluster taken in the 25-pc vicinity of the cluster (the grey area is zoomed in the top-right panel around the value of unity for clarity). The time is relative, with $t = 0$ being the time of first detection. The different colours represent different simulations. The simulation using only radiative feedback is labelled here as Rad feedback. For the simulations with full and radiative feedback, solid lines show clusters (labelled as C1) that keep their gas reservoir, while dashed lines show clusters (labelled as C2) that expel it. *Bottom left*: Evolution of the stellar mass of the clusters during their first 50 Myr. *Bottom right*: Evolution of the mass of the gas reservoir.

in Fig. 5. The energies are computed using the mass, velocities associated with the gaseous cells and stellar particles. The kinetic and thermal energies we calculate are defined respectively as $E_{\rm kin} = 0.5 \sum_i m_i v_i^2$ and $E_{\rm therm} = \frac{1}{M_{\rm tot}} \sum_i 3/2 k_{\rm B} m_i T_i$, where m_i is the mass of the ith gas cell, v_i is its velocity minus the average velocity of the field, T_i is its temperature, $k_{\rm B}$ is the Boltzmann constant, and $M_{\rm tot}$ is the sum of all m_i. The gravitational energy is computed from the gravitational acceleration of the stars and the gas.

In the SN-feedback simulation, the energy from SNe is immediately dissipated, and the gravitational energy dominates (the energy ratio is always lower than unity). Thus, the gas is retained within the close environment of the cluster, which can then slowly grow its stellar mass. Finally, we note that the gas mass within 25 pc is almost a constant, showing that the consumption of gas by star formation is balanced by the accretion of gas.

When we include the radiation feedback, the C1 clusters retain their gas in both the radiative-only and the full feedback cases, despite a bumpier evolution of the total (i.e. stars + gas) energy. During the first 15 Myr, the thermal energy associated with H II regions is deposited into the ISM. Since the mass of the cluster is lower than that of the gas by at least one order of magnitude, internal energy dominates the potential with an energy ratio higher than 1. This ratio then slowly decreases over time, reflecting both the steady growth in stellar mass and the build-up of a massive gas reservoir (the variations of the internal energy are less important than those of the gravitational energy by a factor of 2). The next 35 Myr sees the gravitational energy dominating over the internal energy of the gas, reaching a balance similar to that observed in the SN-only case.

The evolution of the total energy of the C2 clusters is clearly different and linked to their gas environments. After respectively ∼5 and ∼20 Myr, both the stellar and the gas mass of the C2 clusters suddenly drop, the latter by several orders of magnitude. This follows the formation of a bubble around the cluster, which heats the gas. During these few millions of years, the cluster enters a depleted region of (dense) gas in the disc, reducing the chances for the cluster to accrete more material. This leads to a simultaneous decrease of the internal energy of the gas and of the gravitational energy. The relative decrease between these two components determines the outcome energy ratio. For Full-C2, the mass of the gas reservoir significantly decreases after about 18 Myr as the cluster is bathed in a hot (5×10^4 K) ISM. This hot gas is not dense enough to be gravitationally bound to the cluster, and the thermal energy dominates, leading to a significant increase of the energy ratio. For H II-C2, as thermal energy from H II bubbles is deposited

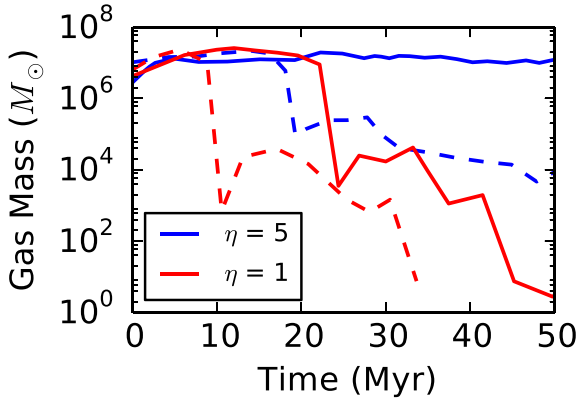

Figure 6. Early evolution of the mass of gas reservoirs in star clusters in simulations using a mass-loading factor η of 5 and 1 (blue and red respectively). In the latter case, the chosen star clusters have survived up to $t = 600$ Myr and lost their reservoir. Time is relative, with $t = 0$ Myr being the time of formation. Each style shows a different star cluster.

into the ISM, the cluster enters a low-density gaseous region of the disc. The gas escapes from the cluster gravitation and the energy ratio decreases dramatically. In both cases, the C2 clusters are almost cleared of their gas reservoirs in a few tens of millions of years, and these are not replenished via accretion from the local environment. Note that the decrease of the gravitational energy of these C2 clusters allows the stars with the highest kinetic velocity to escape.

Similarly to in the SN-only case, we test whether the mass-loading factor from SNe, now coupled with radiative feedback, affects the early evolution of the mass of star clusters. We thus conduct another simulation with all feedback recipes active and set $\eta = 1$. In such conditions, at $t = 600$ Myr, two clusters of $\sim 4 \times 10^5 M_\odot$ without gas reservoirs are detected. We note that no nucleus has formed by that time, in contrast to the reference simulation. The early evolution of the gas reservoir of the two detected clusters is shown in Fig. 6 and compared with the clusters C1 and C2 of the reference simulation.

When the mass-loading factor is 1, the early evolution of both gas reservoirs of star clusters is similar to that of cluster C2 but anticipated by 5 or 10 Myr. We note that the first gas-clearing episode (occurring 10 and 21 Myr after the cluster formation) seems to be more efficient than in the reference simulation by an order of magnitude in mass. An intuitive explanation for this is that a low mass-loading factor brings a larger volume of gas towards lower densities, which then facilitates the dissipation of the gas reservoir by radiative feedback. This shows the impact of the non-linear coupling of different feedback processes (e.g. the radiative feedback and the SNe with the mass-loading of the winds) on gas reservoirs and their potential ability to prevent the growth of massive clusters and NC progenitors. We finally note that, after the first depletion of the reservoir, some amount of gas is brought into the clusters (e.g. small increases of the mass reservoir at $t = 10$ and 29 Myr for the red-dashed cluster). Because the mass-loading factor also changes the velocity of the gas carried in the debris, some gas is able to return to the cluster. However, this gas is not dense enough to form new stars, and the stellar mass of the cluster does not change drastically after the first expulsion.

Overall, the evolution of star clusters is determined by a fragile balance between their own gravity and the physical properties of their gas. SNe seem to play a role only if they are coupled with radiative feedback. The gas density and temperature of the environment in which clusters evolve are major factors that can change the evolution of the gas reservoir. Massive star clusters are likely to grow if their density allows them to keep dense gas bound to them and if they continuously evolve in a dense gas environment during their first tens of millions of years.

4 DISCUSSION AND CONCLUSION

Our use of hydrodynamical simulations of isolated gas-rich galaxies with different radiation feedback setups has enabled us to draw the following conclusions.

(i) SNe alone are (mostly) inefficient at affecting the gas reservoir and the early growth of star clusters. Feedback mechanisms associated with H II regions and radiative pressure seem to have a more significant impact, and are thus important components in the early life stages of star clusters.

(ii) When radiation feedback is included, the growth of star clusters via gas accretion depends on the ability of the cluster to retain and/or replenish calibration gas reservoir. That ability is closely tied to the local environment that the cluster passes through during the first tens of millions of years, and to the corresponding availability of dense gas around the cluster as it orbits within the disc. This allows the galaxy to develop two categories of star cluster populations: those from which feedback expels the gas reservoir shortly after cluster formation, and those in a denser environment around which feedback fails to totally clear the gas. We also note that low mass-loading factors (i.e. 1 in our case) for the SN blast coupled with radiative feedback can efficiently disperse dense gas, thus preventing the growth of star clusters.

(iii) In H II- or full-feedback simulations, we would expect only the massive end of the cluster distribution to survive (with a typical mass of a few 10^5 to a few 10^6 Myr in the present case), depending on the specific locations/trajectories of the clusters.

These conclusions align with those of several studies. Based on time-scale estimations, Krumholz & Matzner (2009) argued that SNe should play a limited role as a source of feedback in star clusters, because H II regions inject their energy immediately after the star formation and do not have delays as is the case for SNe. In addition, results from Li, Bryan & Ostriker (2017) suggest that the impact of SNe is weaker in high-density environments, which is where our clusters form (see their fig. 10). On galactic scales, Butler et al. (2017) showed that the combination of H_2 dissociation, photoionization from extreme ultraviolet photons and SNe leads to different properties of the gas in terms of temperature and different spatial distributions of young stars compared with the case in which only SNe are active. Our experiments point towards the same trends, emphasizing the importance of non-linear multi-component feedback, in particular in the formation of massive stellar objects.

The impact of feedback in numerical simulations obviously depends on the employed subgrid implementations of SN and radiative feedback. Our work suggests that SNe alone are inefficient at disturbing the gas properties and the production of stars (see also Smith et al. 2018). Similar results have been observed when thermal feedback is used: it has been suggested that such inefficiency may be due to the fact that the SN energy is distributed over too much mass, meaning that the temperature of the heated ISM around the SN is too low (Dalla Vecchia & Schaye 2008). A potential measure to stop the gas from over-cooling with only SNe would be to use a mechanical feedback as in Smith et al. (2018), as it injects momentum depending on the relevant scale of the SN remnant. In their work,

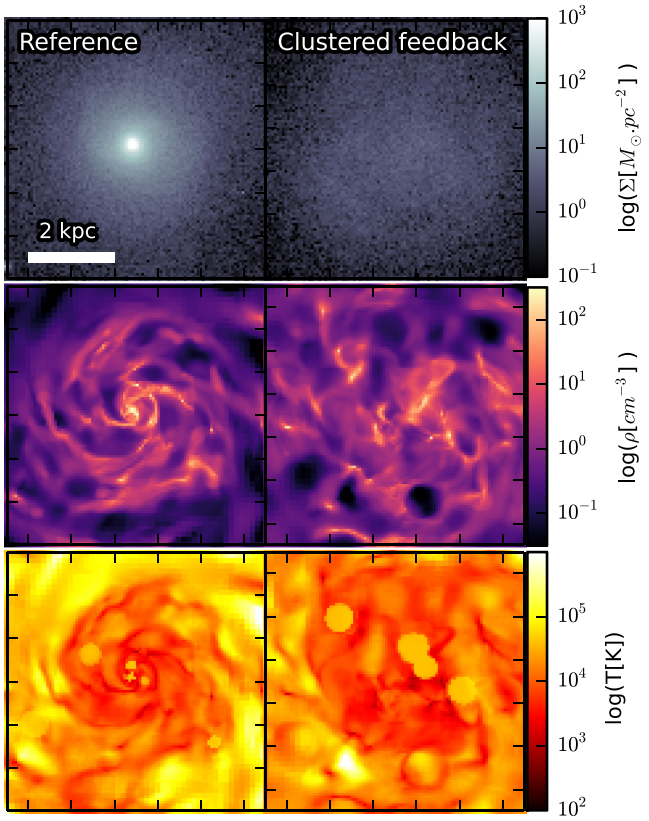

Figure 7. Maps of stellar (*top*) and gas (*middle*) densities and gas temperature (*bottom*) using two feedback setups at $t = 2.5$ Gyr. The left panels show our reference simulation. In the right panels, we generate 10 times fewer H II regions, but each of these is 10 times more energetic (in order to conserve the total energy injected into the ISM of the whole disc). This generates differences in the ISM and star cluster properties, which modify the final morphology of our dwarf galaxy.

Smith et al. (2018) showed that this technique has the advantage of reaching numerical convergence of the star formation rate even at a resolution of 8.1 pc. Nonetheless, it is unclear how the non-linear coupling between this kind of feedback and radiation will affect the properties of the ISM and those of star clusters.

The implementation of the ingredients used for our radiative feedback also plays a role because the properties (size, mass, energy, etc) of H II regions may vary, depending on the local conditions. In a gas-rich environment, such variations could directly impact the star cluster population and its evolution. In order to illustrate this point, we can artificially increase the energy input for individual H II regions while conserving the total injected energy (by lowering the number of H II regions), the radial extent of the associated bubbles increasing accordingly (by a factor of about 10). Because the radius of the bubbles increases, we refer to this setting as clustered feedback.

Fig. 7 illustrates how such an imposed change in the energy injection scheme naturally perturbs the morphology of the galaxy by, ultimately, preventing the formation of a nucleus. Indeed, the local heating by larger H II regions induces a decrease in the local gas density, which alters the density properties on a larger scale (i.e. kiloparsec scales) and with this, the location and number of the forming star cluster sites. Larger gas-rich volumes are heated, and a larger fraction of dense gas is shifted to lower densities, hence compromising the further growth of potential NC progenitors. Hence, calibrating the radiative feedback is of crucial importance when studying the properties of gas in discs and the morphology of galaxies in general. Furthermore, because the effect of radiative feedback depends on the gas density in the disc and thus on the spatial resolution, such a calibration should be different for simulations of isolated discs and cosmological simulations.

Stellar feedback further encompasses several coupled processes other than SN or radiative feedback, some of which are not included in the present simulations (e.g. photoelectric heating, cosmic rays). Discussions on the relative effects of these feedback processes can be found (for dwarf galaxies) in, for example, Kim et al. (2013a,b), Hu et al. (2017) and Forbes et al. (2016). Feedback from low- and intermediate-mass stars could also impose a time delay on star formation (Offner et al. 2009; Dale 2017), thus potentially lowering the number of clusters: such an effect has been ignored in our simulation because we do not sample the initial mass function. Magnetic fields, which could suppress the expansion of H II regions (Krumholz, Stone & Gardiner 2007; Peters et al. 2011), are also not taken into account: their inclusion might enhance the ability of a cluster to grow because a smaller volume would be heated by the bubbles. Finally, cosmic rays are currently thought to be generated by SNe and massive-star winds, which are encountered in regions of massive-star formation (VERITAS Collaboration et al. 2009; Bykov et al. 2017). The heating of the gas from cosmic rays might be an obstacle to a high-density gas reservoir and thus to the growth of NC seeds.

In our simulations, these seeds all reach a mass of $\sim 10^6 M_\odot$ after a few millions of years. High-resolution studies of individual giant molecular clouds (GMCs), such as that by Dale et al. (2012), have shown that clusters above $\sim 10^6 M_\odot$ have a high enough escape velocity to prevent H II regions from efficiently removing gas from the clusters. This further illustrates the potential ability of the young massive clusters in general and NC progenitors in particular to retain their gas reservoirs in dense environments, such as gas-rich galaxies and mergers. On the other hand, the lower-mass clusters ($\lesssim 10^5 M_\odot$) are strongly impacted by ionizing feedback. We also note that the mass range and the parent GMC of our C2 clusters are in agreement with recent work by Howard, Pudritz & Harris (2017), who studied the impact of the inclusion of radiation feedback on the efficiency of cluster formation and established a relationship between the maximum mass of a star cluster and the mass of the parent cloud ($M_{\rm cluster,max} \propto M_{\rm cloud}^{0.81}$).

Most of the clusters we have studied have densities of $\sim 10 M_\odot$ pc^{-3}. Our spatial and mass resolution does not allow us to form low-mass bound systems such as associations and open clusters. The typical stellar density for these objects ranges from 0.01 to 1 star pc^{-3} for associations and open clusters, respectively. This would require a subparsec resolution, which is beyond the scope of this study. Lower-mass clusters (e.g. 10^3–$10^4 M_\odot$) are expected to be more vulnerable to feedback disturbances in a gas-rich environment. Associations generally disperse over time-scales of 10 Myr, and we would expect feedback to contribute to the dissolution process.

Galactic and extragalactic environments are also likely to affect the properties of star clusters, such as their mass or density. Open clusters are mostly observed in spiral arms (Dias et al. 2002), whereas more massive (forming) clusters are observed in for example starbursts and mergers (e.g. Portegies Zwart et al. 2010) or central regions (Böker et al. 2002). For the specific cases of NCs, hosted at the centre of galactic discs, some studies (Emsellem et al. 2015; Torrey et al. 2017) suggest an interplay between star

formation and feedback processes, leading to gas accretion–ejection cycles and possibly to complex integrated star-formation histories (Feldmeier-Krause et al. 2015). In galaxy mergers such as the Antennae, young massive star clusters generate superbubbles spanning hundreds of parsecs (Camps-Fariña et al. 2017) in the nuclear regions, which might remove the least dense gas and hence halt the star formation within these clusters.

Overall, this work emphasizes the importance of the calibration of feedback recipes, its impact on the properties of the ISM and star clusters. We also note the importance of a more realistic galactic-scale environment (interactions, gas accretion) for the early formation and evolution of massive clusters.

ACKNOWLEDGEMENTS

We thank the anonymous referee for her/his helpful comments and suggestions that helped us to improve the paper. We also thank Oscar Agertz for interesting discussions. This research was supported by the DFG cluster of excellence 'Origin and Structure of the Universe' (www.universe-cluster.de). The simulations were carried out on the computing facilities of the Computational Centre for Particle and Astrophysics (C2PAP). FR acknowledges support from the European Research Council through grant ERC-StG-335936 and the Knut and Alice Wallenberg Foundation.

REFERENCES

Agertz O., Kravtsov A. V., 2015, ApJ, 804, 18
Agertz O., Kravtsov A. V., 2016, ApJ, 824, 79
Agertz O., Kravtsov A. V., Leitner S. N., Gnedin N. Y., 2013, ApJ, 770, 25
Arca-Sedda M., Capuzzo-Dolcetta R., Antonini F., Seth A., 2015, ApJ, 806, 220
Audit E., Hennebelle P., 2010, A&A, 511, A76
Bekki K., 2017, MNRAS, 467, 1857
Böker T., Laine S., van der Marel R. P., Sarzi M., Rix H.-W., Ho L. C., Shields J. C., 2002, AJ, 123, 1389
Bournaud F., Elmegreen B. G., Teyssier R., Block D. L., Puerari I., 2010, MNRAS, 409, 1088
Butler M. J., Tan J. C., Teyssier R., Rosdahl J., Van Loo S., Nickerson S., 2017, ApJ, 841, 82
Bykov A. M., Ellison D. C., Gladilin P. E., Osipov S. M., 2017, preprint, (arXiv:1706.01135)
Camps-Fariña A., Zaragoza-Cardiel J., Beckman J. E., Font J., Velázquez P. F., Rodríguez-González A., Rosado M., 2017, MNRAS, 467, 4134
Carollo C. M., Stiavelli M., Mack J., 1998, AJ, 116, 68
Chatterjee S., Rodriguez C. L., Rasio F. A., 2017, ApJ, 834, 68
Cole D. R., Debattista V. P., 2016, Galactic Bulges, 418, 107
Daddi E. et al., 2010, ApJ, 713, 686
Dale J. E., 2017, MNRAS, 467, 1067
Dale J. E., Ercolano B., Bonnell I. A., 2012, MNRAS, 424, 377
Dalla Vecchia C., Schaye J., 2008, MNRAS, 387, 1431
den Brok M. et al., 2014, MNRAS, 445, 2385
Dias W. S., Alessi B. S., Moitinho A., Lépine J. R. D., 2002, A&A, 389, 871
Dubois Y., Teyssier R., 2008, A&A, 477, 79
Eisenstein D. J., Hut P., 1998, ApJ, 498, 137
El-Badry K., Wetzel A., Geha M., Hopkins P. F., Kereš D., Chan T. K., Faucher-Giguère C.-A., 2016, ApJ, 820, 131
Emsellem E., Renaud F., Bournaud F., Elmegreen B., Combes F., Gabor J. M., 2015, MNRAS, 446, 2468
Feldmeier-Krause A. et al., 2015, A&A, 584, A2
Ferrero I., Abadi M. G., Navarro J. F., Sales L. V., Gurovich S., 2012, MNRAS, 425, 2817
Forbes J. C., Krumholz M. R., Goldbaum N. J., Dekel A., 2016, Nature, 535, 523
Geach J. E. et al., 2014, Nature, 516, 68
Geen S., Hennebelle P., Tremblin P., Rosdahl J., 2016, MNRAS, 463, 3129
Gies D. R., 1987, ApJS, 64, 545
Grisdale K., Agertz O., Romeo A. B., Renaud F., Read J. I., 2017, MNRAS, 466, 1093
Guillard N., Emsellem E., Renaud F., 2016, MNRAS, 461, 3620
Hayward C. C., Hopkins P. F., 2017, MNRAS, 465, 1682
Hopkins P. F., Kereš D., Oñorbe J., Faucher-Giguère C.-A., Quataert E., Murray N., Bullock J. S., 2014, MNRAS, 445, 581
Hopkins P. F. et al., 2017, preprint (arXiv:1702.06148)
Howard C. S., Pudritz R. E., Harris W. E., 2016, MNRAS, 461, 2953
Howard C., Pudritz R., Harris W., 2017, MNRAS, 470, 3346
Hu C.-Y., Naab T., Glover S. C. O., Walch S., Clark P. C., 2017, MNRAS, 471, 2151
Kim J.-h., Krumholz M. R., Wise J. H., Turk M. J., Goldbaum N. J., Abel T., 2013a, ApJ, 775, 109
Kim J.-h., Krumholz M. R., Wise J. H., Turk M. J., Goldbaum N. J., Abel T., 2013b, ApJ, 779, 8
Krumholz M. R., Matzner C. D., 2009, ApJ, 703, 1352
Krumholz M. R., Stone J. M., Gardiner T. A., 2007, ApJ, 671, 518
Krumholz M. R. et al., 2014, in Beuther H., Klessen R. S., Dullemond C. P.,Henning T., eds, Protostars and Planets VI. Univ. Arizona Press, Tucson, p. 243
Lada C. J., Lada E. A., 2003, ARA&A, 41, 57
Lamers H. J. G. L. M., Kruijssen J. M. D., Bastian N., Rejkuba M., Hilker M., Kissler-Patig M., 2017, A&A, 606, A85
Lee Y.-W., Joo J.-M., Sohn Y.-J., Rey S.-C., Lee H.-C., Walker A. R., 1999, Nature, 402, 55
Leitherer C. et al., 1999, ApJS, 123, 3
Li C.-Y., de Grijs R., Deng L.-C., 2016, Res. Astron. Astrophys., 16, 179
Li M., Bryan G. L., Ostriker J. P., 2017, ApJ, 841, 101
Longmore S. N. et al., 2014, in Beuther H., Klessen R. S., Dullemond C.P., Henning T. K., eds, Protostars and Planets VI. Univ. Arizona Press, Tucson, p. 291
Lopez L. A., Krumholz M. R., Bolatto A. D., Prochaska J. X., Ramirez-Ruiz E., 2011, ApJ, 731, 91
Mac Low M.-M., Klessen R. S., 2004, Rev. Mod. Phys., 76, 125
MacLachlan J. M., Bonnell I. A., Wood K., Dale J. E., 2015, A&A, 573, A112
Meurer G. R., Heckman T. M., Leitherer C., Kinney A., Robert C., Garnett D. R., 1995, AJ, 110, 2665
Milosavljević M., 2004, ApJ, 605, L13
Naab T., Ostriker J. P., 2017, ARA&A, 55, 59
Navarro J. F., Frenk C. S., White S. D. M., 1996, ApJ, 462, 563
Nelson D., Genel S., Vogelsberger M., Springel V., Sijacki D., Torrey P., Hernquist L., 2015, MNRAS, 448, 59
Niederhofer F., Bastian N., Kozhurina-Platais V., Hilker M., de Mink S. E., Cabrera-Ziri I., Li C., Ercolano B., 2016, A&A, 586, A148
Núñez A., Ostriker J. P., Naab T., Oser L., Hu C.-Y., Choi E., 2017, ApJ, 836, 204
Offner S. S. R., Klein R. I., McKee C. F., Krumholz M. R., 2009, ApJ, 703, 131
Parker R. J., Goodwin S. P., 2007, MNRAS, 380, 1271
Perets H. B., Mastrobuono-Battisti A., 2014, ApJ, 784, L44
Peters T., Banerjee R., Klessen R. S., Mac Low M.-M., 2011, ApJ, 729, 72
Pfeffer J., Griffen B. F., Baumgardt H., Hilker M., 2014, MNRAS, 444, 3670
Portegies Zwart S. F., McMillan S. L. W., Gieles M., 2010, ARA&A, 48, 431
Raskutti S., Ostriker E. C., Skinner M. A., 2016, ApJ, 829, 130
Renaud F. et al., 2013, MNRAS, 436, 1836
Rey-Raposo R., Dobbs C., Agertz O., Alig C., 2017, MNRAS, 464, 3536
Rossa J., van der Marel R. P., Böker T., Gerssen J., Ho L. C., Rix H.-W., Shields J. C., Walcher C.-J., 2006, AJ, 132, 1074

Seth A. C., Dalcanton J. J., Hodge P. W., Debattista V. P., 2006, AJ, 132, 2539
Smith M. C., Sijacki D., Shen S., 2018, MNRAS, in press
Teyssier R., 2002, A&A, 385, 337
Torrey P., Hopkins P. F., Faucher-Giguère C.-A., Vogelsberger M., Quataert E., Kereš D., Murray N., 2017, MNRAS, 467, 2301
Tremaine S. D., Ostriker J. P., Spitzer L., Jr, 1975, ApJ, 196, 407
Tremblin P. et al., 2014, A&A, 568, A4
VERITAS Collaboration et al., 2009, Nature, 462, 770
Walch S. K., Whitworth A. P., Bisbas T., Wünsch R., Hubber D., 2012, MNRAS, 427, 625
Wareing C. J., Pittard J. M., Falle S. A. E. G., 2017, MNRAS, 470, 2283

This paper has been typeset from a TEX/LATEX file prepared by the author.